Inorganic Chemistry

Article

pubs.acs.org/IC

Supramolecular Rotators of (Aniliniums)([18]crown-6) in Electrically Conducting [Ni(dmit)$_2$] Crystals

Norihisa Hoshino,[†,‡] Yuuya Yoshii,[‡] Masaki Aonuma,[∥] Kazuya Kubo,[§,∥] Takayoshi Nakamura,*[,§,∥] and Tomoyuki Akutagawa*[,†,‡]

[†]Institute of Multidisciplinary Research for Advanced Materials (IMRAM), Tohoku University, Katahira 2-1-1, Aoba-ku, Sendai 980-8577, Japan

[‡]Graduate School of Engineering, Tohoku University, Sendai 980-8579, Japan

[§]Research Institute for Electronic Science, Hokkaido University, Sapporo 060-0812, Japan

[∥]Graduate School of Environmental Science, Hokkaido University, Sapporo 060-0810, Japan

Supporting Information

ABSTRACT: Supramolecular assemblies of anilinium (Ani$^+$) and fluoroanilinium derivatives (FAni$^+$) with [18]crown-6 were introduced into electrically conducting [Ni(dmit)$_2$] crystals (dmit^{2-} is 2-thioxo-1,3-dithiole-4,5-dithiolate). The crystal structures, electrical conductivities, and magnetic susceptibilities of four new crystals of (Ani$^+$)([18]crown-6)[Ni(dmit)$_2$]$_3$ (**1**), (*o*-FAni$^+$)([18]crown-6)[Ni(dmit)$_2$]$_3$ (**2**), (*m*-FAni$^+$)([18]crown-6)[Ni(dmit)$_2$]$_3$ (**3**), and (*p*-FAni$^+$)([18]crown-6)[Ni(dmit)$_2$]$_3$ (**4**) were examined from the viewpoint of dynamic supramolecular rotator structures within the crystals. The crystal structures, electrical conduction, and magnetic properties were classified into group-**I** (crystals **1** and **4**) and group-**II** (crystals **2** and **3**). The hydrogen-bonding interaction between -NH$_3^+$ and the oxygen atoms of [18]crown-6 formed the stand-up configuration of rotator-stator structures of (Ani$^+$)([18]crown-6) and (FAni$^+$)([18]crown-6) supramolecules. The potential energy barriers for the 2-fold flip-flop motion of phenyl- and *p*-fluorophenyl-rings in crystals **1** and **4** had a relatively small magnitude of ∼150 kJmol^{-1}, suggesting that rotations of Ani$^+$ and *p*-FAni$^+$ cations around the C-NH$_3^+$ axis occurred in the crystals. In contrast, a large magnitude of the potential energy barriers for the rotations of *o*-FAni$^+$ and *m*-FAni$^+$ cations in crystals **2** and **3** (>600 kJmol^{-1}) resulted in static supramolecular cationic structures. The cation:anion ratio of 1:3 in these crystals yielded a trimer π-stack of [Ni(dmit)$_2$] with a semiconductor-like temperature dependence. The magnetic susceptibilities of the static crystals **2** and **3** were reproduced by the one-dimensional antiferromagnetic linear Heisenberg chain through the one-dimensional linear trimer arrangement. The magnetic susceptibilities of dynamic crystals **1** and **4** enhanced electron delocalization through the intratrimer and intertrimer interactions within the trimer stack, where the molecular rotations of Ani$^+$ and *p*-FAni$^+$ cations played an important role.

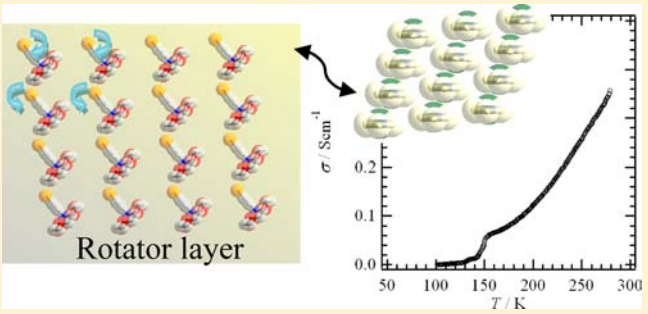

INTRODUCTION

A variety of functional π-planar molecular materials, electrically conducting and with magnetic properties, have been investigated for future applications in flexible organic electronics.[1] One of the notable points of these molecular materials is the diversity of molecular designs for various molecular arrangements in assemblies and desirable physical functionalities such as electrical conductivity, magnetic properties, and optical properties.[1,2] In electrically conducting molecular materials, electrical band structures are directly determined by the overlap of frontier-orbitals (LUMO and/or HOMO), resulting in a variety of electronic ground states, from semiconducting to metallic to superconducting, depending on the dimensionality, band-filling, and electron correlations.[2] The monovalent radical cation and/or anion state of π-molecules has one S = 1/2 spin on the molecule, localized on the molecule because of the large magnitude of the on-site Coulomb repulsive energy (U) of a typical organic π-molecule.[3] However, the $\pi-\pi$ interactions between monovalent radical molecules yielded magnetic exchange energy between the localized S = 1/2 spins, resulting in bulk magnetic properties. A large number of electrically active π-molecules such as tetrathiafulvalene (TTF), 7,7,8,8-tetracyano-*p*-quinodimethane (TCNQ), fullerene (C_{60}), and [Ni(dmit)$_2$] (dmit^{2-} is 2-thioxo-1,3-dithiole-4,5-dithiolate) have been utilized as building blocks of electrically conducting and magnetic molecular materials.[2,3] Since the bandwidth (W) of molecular crystals is smaller than that of typical inorganic metals, one electron on the frontier orbital has a tendency to localize in the crystal because of a large magnitude of U.[3] A

Received: September 27, 2012
Published: November 20, 2012

   dx.doi.org/10.1021/ic302093b | *Inorg. Chem.* 2012, 51, 12968−12975

partially filled π-band is required for high electrical conduction, whereas the monovalent electronic states of cation and/or anion radical species yield localized $S = 1/2$ spin in the crystals. Among diverse electrically active π-molecules, we noticed the electrically conducting and magnetic $[Ni(dmit)_2]$ crystal ($dmit^{2-}$ is 2-thioxo-1,3-dithiole-4,5-dithiolate). According to the oxidized state and packing structures of $[Ni(dmit)_2]$ molecules, a variety of physical properties from superconducting, metallic, semiconducting, to insulator have been reported in crystalline states.[4]

We have been utilizing a supramolecular cation approach to design the electrical conducting and magnetic properties of $[Ni(dmit)_2]$ crystals.[5−9] The (cation)(crown ethers) molecular-assemblies have structural diversity in terms of the assembly structure, exclusive volume, and valence, and are easily prepared by a combination of a variety of cations and crown ethers. The supramolecular cations are introduced into the monovalent and/or partially oxidized $[Ni(dmit)_2]$ crystals as functional counter cations, where the structural flexibility and dynamic properties of supramolecular cations play an important role to yield new additional functionalities. For instance, ionic channel structures have been constructed in one-dimensional arrays of [15]crown-5 and [18]crown-6 in electrically conducting $Li^+_x([15]crown\text{-}5)[Ni(dmit)_2]_2$ and $Li^+_{0.7}([18]crown\text{-}6)[Ni(dmit)_2]_2$ crystals,[5a,b] wherein the electrical conductivities were modulated by the motional freedom of the Li^+ ions. Thermally activated rotation of [18]crown-6 has been observed in the $Cs^+_2([18]crown\text{-}6)_3[Ni(dmit)_2]_2$ crystal, where the magnetic susceptibility of a single-triplet thermal excitation model was affected by the molecular rotation of [18]crown-6 around 220 K.[7] Uniaxial rotations of anilinium (Ani^+), adamantylammonium ($ADNH_3^+$), and *m*-fluoroanilinium (*m*-$FAni^+$) along the C-NH_3^+ axis have been designed in monovalent $[Ni(dmit)_2]^-$ crystals (Scheme 1).[8,9] Among these, the thermally activated 2-fold flip-flop motion of *m*-$FAni^+$ in the (*m*-$FAni^+$)(dibenzo[18]crown-6)$[Ni(dmit)_2]^-$ crystal resulted in dipole inversion, exhibiting the ferroelectric-paraelectric phase transition around 350 K.[9] Although molecular rotations in molecular crystals are well-known phenomena in plastic crystalline states, the ferroelectric property can be directly associated with molecular rotation in the (*m*-$FAni^+$)(dibenzo[18]crown-6)$[Ni(dmit)_2]^-$ crystal.

Scheme 1. Molecular Structures of Fluoroanilinium ($FAni^+$), [18]crown-6, and $[Ni(dmit)_2]$

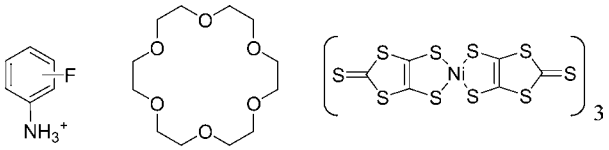

$FAni^+$ [18]crown-6 $[Ni(dmit)_2]^-$

EXPERIMENTAL SECTION

Preparation of $[Ni(dmit)_2]^-$ Crystals. Single crystals of **1**−**4** were prepared by the standard electrocrystallization method in an H-shaped cell (~20 mL). The supporting electrolytes of (Ani^+)(BF_4^-), (*o*-$FAni^+$)(BF_4^-), (*m*-$FAni^+$)(BF_4^-), and (*p*-$FAni^+$)(BF_4^-) for crystals **1**−**4**, respectively, were prepared from 54% aqueous tetrafluoroboric acid (HBF_4) and aniline derivatives in a CH_3CN−CH_2Cl_2 mixed solvent (Supporting Information, Table S1). A green solution of (*n*-Bu_4N)$[Ni(dmit)_2]$ (15 mg) in CH_3CN (~10 mL) was inserted into one side of the electrocrystallization cell, while a solution of supporting electrolyte (~30 mg) and [18]crown-6 (~150 mg) in CH_3CN (~10 mL) (detailed conditions of the single crystal preparation are shown in Supporting Information, Table S2) was poured into the other side of the cell. A constant current of 1 μA was applied to the platinum electrodes (1 mm ϕ) for two weeks at room temperature, which yielded black platelet single crystals with dimensions of $0.4 \times 0.3 \times 0.1$ mm^3. The stoichiometry of the crystals was determined by X-ray structural and elemental analyses. Elemental analysis of crystal **1**: Calcd for $C_{36}H_{32}NO_6S_{30}Ni_3$: C, 25.25; H, 1.88; N, 0.82. Found. C, 24.80; H, 2.06; N, 0.89. Crystal **2**: Calcd for $C_{36}H_{31}NO_6FS_{30}Ni_3$: C, 24.98; H, 1.81; N, 0.81. Found. C, 24.84; H, 1.95; N, 0.79. Crystal **3**: Calcd for $C_{36}H_{31}NO_6FS_{30}Ni_3$: C, 24.98; H, 1.81; N, 0.81. Found. C, 25.51; H, 2.07; N, 0.93. Crystal **4**: Calcd for $C_{36}H_{31}NO_6FS_{30}Ni_3$: C, 24.98; H, 1.81; N, 0.81. Found. C, 24.80; H, 1.89; N, 0.79.

Crystal Structure Determination. Crystallographic data (Table 1) were collected by a Rigaku RAXIS-RAPID diffractometer using Mo−Kα (λ = 0.71073 Å) radiation from a graphite monochromator. Structure refinements were carried out using the full-matrix least-squares method on F^2. Calculations were performed using the Crystal Structure and SHELX software packages.[10] Parameters were refined using anisotropic temperature factors except for the hydrogen atom.

Calculations. The relative energy of the model structures was calculated using the RHF/6-31(*d*) basis set.[11] The nearest-neighboring molecules around the phenyl- and fluorophenyl-rings of Ani^+ and $FAni^+$ were included in the calculations of the potential energy curves. The calculated structures of crystals **1**, **2**, **3**, and **4** were $(Ani^+)_2([18]crown\text{-}6)_2[Ni(dmit)_2]_2$, $(o\text{-}FAni^+)_2(DCH[18]crown\text{-}6)_2[Ni(dmit)_2]$, $(m\text{-}FAni^+)_2([18]crown\text{-}6)_2[Ni(dmit)_2]_2$, and $(p\text{-}FAni^+)_2([18]crown\text{-}6)_2[Ni(dmit)_2]_2$, respectively (see Supporting Information, Figure S7). The atomic coordinates of crystals **1**−**4** based on X-ray crystal structure analyses were used for the calculations. The relative energy of the model structures was obtained by evaluating the rigid rotation of Ani^+ and/or $FAni^+$ around the C-NH_3^+ bond. Rotations were performed every 30°, and the relative energies were calculated using fixed atomic coordinates. The transfer integrals (t) between the $[Ni(dmit)_2]$ anions were calculated within the tight-binding approximation using the extended Hückel molecular orbital method. The lowest unoccupied molecular orbital (LUMO) of the $[Ni(dmit)_2]^-$ molecule was used as the basis function.[12] Semiempirical parameters for Slater-type atomic orbitals were obtained from the literature.[12] The t-value for each pair of molecules was assumed to be proportional to the overlap integral (S) via the equation $t = -10S$ eV.

Electrical Conductivity. The temperature dependent electrical conductivity was measured by the direct current (dc) four-probe method along the long-axis of the crystal. The stacking direction of the $[Ni(dmit)_2]$ molecules was in accordance with the long axis of the crystal. Electrical contacts were prepared using gold paste to attach 10 μm ϕ gold wires to the crystals (Tokuriki 8560).

Magnetic Susceptibility. The temperature-dependent magnetic susceptibility and the magnetization-magnetic field dependence were measured using a Quantum Design MPMS-XL5 SQUID magnetometer using polycrystalline samples. The applied magnetic field was 1 T for all of the temperature-dependent measurements.

RESULTS AND DISCUSSION

Electrocrystallization of (*n*-Bu_4N^+)$[Ni(dmit)_2]^-$ in the presence of corresponding anilinium (Ani^+), *o*-fluoroanilinium (*o*-$FAni^+$), *m*-fluoroanilinium (*m*-$FAni^+$), and *p*-fluoroanilinium (*p*-$FAni^+$), and [18]crown-6 in CH_3CN yielded partially oxidized $[Ni(dmit)_2]$ crystals of (Ani^+)$([18]crown\text{-}6)[Ni(dmit)_2]_3$ (**1**), (*o*-$FAni^+$)$([18]crown\text{-}6)[Ni(dmit)_2]_3$ (**2**), (*m*-$FAni^+$)$([18]crown\text{-}6)[Ni(dmit)_2]_3$ (**3**), and (*p*-$FAni^+$)$([18]crown\text{-}6)[Ni(dmit)_2]_3$ (**4**). 1:1 adducts of supramolecular cations between anilinium derivatives and [18]crown-6 were constructed by six N−H^+∼O hydrogen-bonding interactions, forming a stand-up configuration of the C-NH_3^+ bond of the phenyl-ring with respect to the mean O6-oxygen plane of [18]crown-6. The cation:anion ratio of 1:3 corresponded to the

dx.doi.org/10.1021/ic302093b | Inorg. Chem. 2012, 51, 12968−12975

Table 1. Crystal Data, Data Collection, and Reduction Parameters of Crystals 1−4

	1	2	3	4
chemical formula	$C_{36}H_{32}NO_6$ $S_{30}Ni_3$	$C_{36}H_{31}NO_6NF$ Ni_3S_{30}	$C_{36}H_{31}NO_6N$ FNi_3S_{30}	$C_{36}H_{31}NO_6NF$ Ni_3S_{30}
formula weight	1712.55	1730.54	1730.54	1730.54
space group	$P\bar{1}$ (#2)	$P\bar{1}$ (#2)	$P\bar{1}$ (#2)	$P\bar{1}$ (#2)
a, Å	10.045(2)	11.239(5)	11.350(6)	10.073(2)
b, Å	12.702(2)	12.721(7)	12.831(7)	12.713(2)
c, Å	24.454(4)	24.14(1)	24.10(2)	24.452(4)
α, deg	100.014(2)	78.76(2)	79.78(2)	99.369(5)
β, deg	95.649(2)	83.38(2)	83.85(2)	95.610(4)
γ, deg	95.442(2)	66.75(2)	68.84(2)	96.405(4)
V, Å^3	3037.6(9)	3108(3)	3112(3)	3048.6(8)
Z	2	2	2	2
D_{calc}, g·cm^{-1}	1.872	1.849	1.847	1.885
T, K	173	173	173	173
μ, cm^{-1}	19.960	19.543	19.518	19.921
reflections measured	29489	30338	28792	28901
independent reflections	17122	14085	13634	13661
reflections used	13118	14085	13634	13661
R_1[a]	0.0665	0.0620	0.0456	0.0566
$wR_2(F^2)$[a]	0.0718	0.2183	0.1724	0.1727

[a] $R = \sum||F_o| - |F_c||/\sum|F_o|$ and $R_w = (\sum\omega|F_o| - |F_c|)^2/\sum\omega F_o^2)^{1/2}$.

partially oxidized electronic state of [Ni(dmit)$_2$] in crystals **1**−**4**. Since the unit cell parameters of crystals **1**−**4** resemble each other (Table 1), the same type of segregated stacking structure was observed in all crystals. Crystals **1** and **4** could be classified as the same crystal group-**I**, whereas crystals **2** and **3** were in the same crystal group-**II**, based on the cation−anion arrangements and physical properties.

Cation Conformations. In crystals **1**−**4**, one kind of (anilinium)([18]crown-6) unit was the crystallographically independent structural unit. Figure 1 shows the neighboring pair of each (Ani$^+$)([18]crown-6), (*o*-FAni$^+$)([18]crown-6), (*m*-FAni$^+$)([18]crown-6), and (*p*-FAni$^+$)([18]crown-6) in crystals **1**−**4**. Since the angle between the π-plane of the phenyl-ring and the mean O6-plane of [18]crown-6 in crystals **1**, **2**, **3**, and **4** was 98.0, 95.8, 97.7, and 98.6°, respectively, the phenyl-rings of Ani$^+$ and FAni$^+$ cations were nearly perpendicular to the mean O6-plane of [18]crown-6. The average hydrogen-bonding N∼O distances between the nitrogen and six oxygen atoms of [18]crown-6 in crystals **1**, **2**, **3**, and **4** were 2.92, 2.95, 2.90, and 2.89 Å, respectively, which were comparable to the standard N−H$^+$∼O hydrogen bond distance.[13] Since orientational disorder of the fluorine atom in (*o*-FAni$^+$)([18]crown-6) and (*m*-FAni$^+$)([18]crown-6) in crystals **2** and **3** was not observed in structural analyses at 173 and 298 K, flip-flop motions of the *o*-FAni$^+$ and *m*-FAni$^+$ cations did not occur in these crystals. The flip-flop motions of Ani$^+$ and *p*-FAni$^+$ cations could not be observed in the X-ray crystal structural analyses.

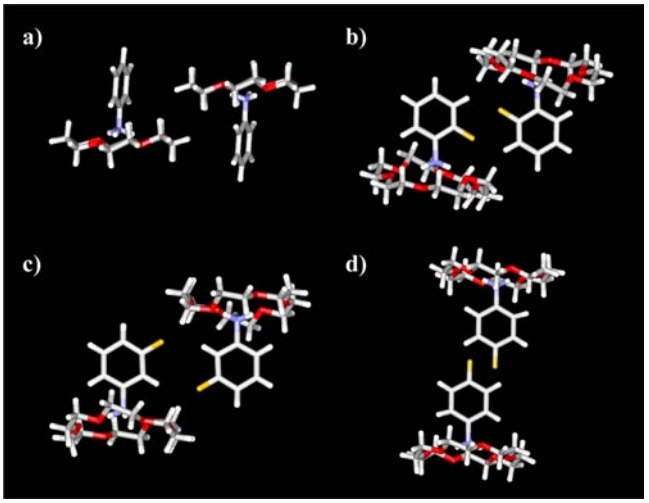

Figure 1. Supramolecular cation structures and neighboring cationic units of (a) (Ani$^+$)([18]crown-6) in crystal **1**, (b) (*o*-FAni$^+$)([18]-crown-6) in crystal **2**, (c) (*m*-FAni$^+$)([18]crown-6) in crystal **3**, and (d) (*p*-FAni$^+$)([18]crown-6) in crystal **4**.

The effective intermolecular interaction between the (Ani$^+$)-([18]crown-6) units was not observed in crystal **1**, similar to that in the monovalent (Ani$^+$)([18]crown-6)[Ni(dmit)$_2$]$^-$ crystal.[8a] The neighboring (FAni$^+$)([18]crown-6) supramolecules interacted through the dipole−dipole interaction of the fluorine atoms. The C−F bonds of each FAni$^+$ cation between the neighboring units were parallel to each other. Since the F−F distances of neighboring *o*-FAni$^+$, *m*-FAni$^+$, and *p*-FAni$^+$ cations were 3.12(2), 3.574(9), and 3.076(5) Å, respectively, the dipole−dipole interactions between the *o*-FAni$^+$ and *p*-FAni$^+$ cations in crystals **2** and **4** were larger than that in crystal **3**. In the case of the (*m*-FAni$^+$)(dibenzo[18]crown-6)[Ni-(dmit)$_2$]$^-$ crystal, the dynamic orientational disorder of the fluorine-group resulted in dipole inversion for the ferroelectric-paraelectric phase transition around 350 K.[9] The dipole−dipole interaction between *m*-FAni$^+$ cations was disturbed by the bulky dibenzo[18]crown-6 molecule, forming sufficient crystalline space for dynamic molecular motion of the *m*-FAni$^+$ cation even in the crystal. The fixed cationic arrangement of *m*-FAni$^+$ through effective dipole−dipole interactions resulted in a static crystal without the molecular rotations.

Cation−Anion Packing Structures. The 1:3 cation−anion ratio and segregated π-stack were consistent with the mixed-valence electronic structure of [Ni(dmit)$_2$] anions and the electrical conducting properties of crystals **1**−**4**. Three kinds of [Ni(dmit)$_2$] (**A**, **B**, and **C**) were the crystallographically independent structural units in these crystals.

dx.doi.org/10.1021/ic302093b | *Inorg. Chem.* 2012, 51, 12968−12975

Although similar two-dimensional $[Ni(dmit)_2]$ layers were observed in crystals **1**−**4**, the magnitude of intermolecular interactions between the $[Ni(dmit)_2]$ anions was modulated by structural differences in the supramolecular cations. The transfer integrals (t) based on extended Hückel molecular orbital calculations were utilized to evaluate the magnitude of the intermolecular interactions between $[Ni(dmit)_2]$ anions within the crystals.[12] Table 2 summarizes the selected transfer integrals of crystals **1**−**4**.

Table 2. Selected Transfer Integrals (t, meV) between the $[Ni(dmit)_2]$ in the *ab*-Plane of Crystals 1−4 (T = 173 K)[a]

	1	2	3	4
t_1	201	−141	145	220
t_2	−200	−178	169	−210
t_3	−17.2	−15.9	13.5	−14.7
t_4	16.4	−47.2	−61.9	15.4
t_5	−25.8			−18.9
t_6	23.5			19.3

[a]Transfer integrals were calculated from the LUMO of $[Ni(dmit)_2]$ based on the extended Hückel calculation (t = −10S eV, S is the overlap integral). t-values larger than 5 meV are summarized.

Since the packing structures of supramolecular cations and $[Ni(dmit)_2]$ in crystals **1**−**4** were almost the same (see unit cell parameters in Table 1), we describe the cation−anion arrangements in crystal **4**. Figures 2a and 2b show the unit

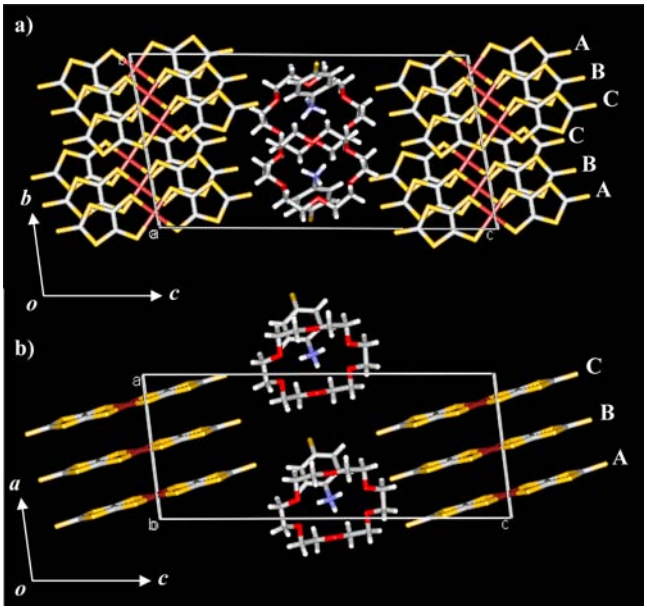

Figure 2. Unit cells of crystal **4** viewed (a) along the *a*-axis and (b) *b*-axis. One (p-FAni$^+$)([18]crown-6) and three $[Ni(dmit)_2]$ (**A**, **B**, and **C**) are crystallographically independent structural units.

cells of crystal **4** viewed along the *a*- and *b*-axis, respectively. The segregated cation−anion arrangement was elongated along the *c*-axis, where the π-stacking structure of $[Ni(dmit)_2]$ and two-dimensional cationic layer were observed. Three kinds of $[Ni(dmit)_2]$ (**A**, **B**, and **C**) formed the π-stacking structure along the *a*+*b* axis. The lateral S∼S contacts between the $[Ni(dmit)_2]$ formed the two-dimensional conducting layer within the *ab*-plane (Figure 2a), where the supramolecular cationic layer was sandwiched by the electrical conducting two-dimensional $[Ni(dmit)_2]$ layers.

$[Ni(dmit)_2]$ Layer. Alternate cation−anion arrangements along the *c*-axis in crystals **1**−**4** were the common structural feature. In all crystals, the electrically conducting two-dimensional $[Ni(dmit)_2]$-layer was observed within the *ab*-plane. Figures 3a and 3b summarize the two types of

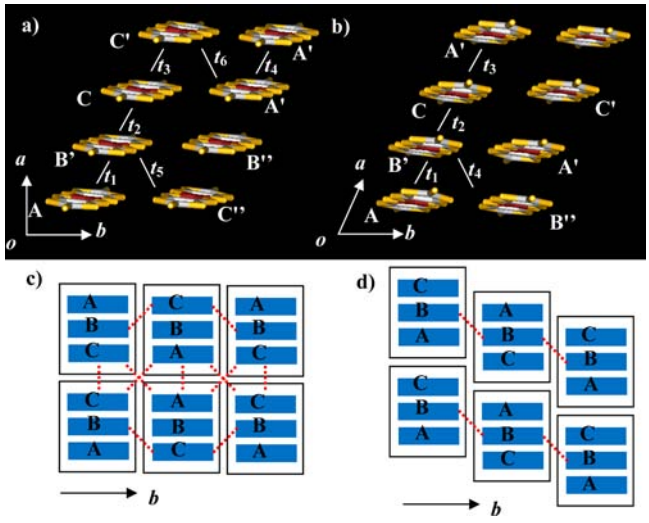

Figure 3. Two-dimensional $[Ni(dmit)_2]$ arrangements in (a) crystals **1**, **4** (group-**I**) and (b) crystals **2**, **3** (group-**II**) viewed along the *c*-axis. Selective intermolecular transfer integrals (t) are shown in the figures. Schematic **A**-**B**-**C** trimer arrangement of (c) crystals **1**, **4** (group-**I**) and (d) crystals **2**, **3** (group-**II**) within the *ab*-plane. Effective intertrimer interactions (red-colored dashed lines) were observed in the crystals.

$[Ni(dmit)_2]$ arrangements in crystals **1**−**4**. From comparison of the t-values, it is seen that the $[Ni(dmit)_2]$ arrangements in crystals **1** and **4** (group-**I**) are different from those in crystals **2** and **3** (group-**II**). The π-stack -**A**-**B**-**C**-**C**′-**B**′-**A**′- in crystals **1** and **4** was observed along the *a*+*b*-axis, where lateral S∼S contacts were observed along the *b*-axis. The π-stacks in crystals **2** and **3** were arranged in the order of -**A**-**B**-**C**-**A**′-**B**′-**C**′- along the *a*-axis, where the lateral S∼S contacts were elongated along the *b*-axis. Along the lateral S∼S contacts, the **B**-**B**′ arrangements in crystal **2** and **3** were different from those in crystals **1** and **4**, where the π-planes of the **B**- and **B**′-units exist on the same plane (Figure 3a).

The formation of strong **A**-**B**-**C** trimers in crystals **1**−**4** was confirmed by the calculations of intratrimer transfer integrals of t_1 and t_2, corresponding to the **A**-**B** and **B**-**C** interactions, respectively. The strong **A**-**B**-**C** trimer was observed in crystals **1** and **4**, where the t_1-interactions of crystals **1** (201 meV) and **4** (220 meV) were almost the same as the t_2-interactions of crystals **1** (−200 meV) and **4** (−210 meV). The t_1-interactions (**A**-**B** pair) of crystals **2** and **3** were −178 and 145 meV, respectively, the magnitude of which is slightly smaller than the t_2-interactions (**B**-**C** pair) of −178 and −169 meV for crystals **2** and **3**, respectively. The intertrimer t_3- and t_4-interactions of **C**-**C**′ and **A**-**A**′ in crystal **1** were −17.2 and 16.4 meV, whereas those in crystal **4** were 15.4 and −18.9 meV, respectively. The t_3- and t_4-interactions in crystals **1** and **4** were 1 order of magnitude smaller than those of the intratrimer interactions. The intertrimer t_3-interactions of **C**-**A**′ in crystals **2** and **3** were −15.9 and 13.5, respectively, 1 order of magnitude smaller than those of the intratrimer interactions. The **A**−**B**-**C** trimers were

dx.doi.org/10.1021/ic302093b | Inorg. Chem. 2012, 51, 12968−12975

isolated with respect to each other in the one-dimensional π-stack of [Ni(dmit)$_2$]. Besides weak lateral interactions less than 5 meV along the *b*-axis, effective lateral t_4-interactions of −47.2 and −61.9 meV were observed in the **B**-**B**′ pair of crystals **2** and **3** along the *-a+b* axis, respectively. The effective S∼S contacts in crystals **1** and **4** were also observed at t_S = 23.5 and 19.3 meV of the **B**-**C**′ pair along the *-a+b* axis. Figures 3c and 3d show a schematic representation of the **A**-**B**-**C** trimer arrangements of group-**I** (crystals **1** and **4**) and group-**II** (crystals **2** and **3**), respectively. The effective intertrimer interactions through the lateral S∼S contacts are indicated by red-colored dashed lines. From the charged state of [Ni(dmit)$_2$], one electron with S = 1/2 spin was located on each **A**-**B**-**C** trimer. Therefore, the magnetic exchange energies in crystals **1**−**4** were governed by the intertrimer interactions within the two-dimensional [Ni(dmit)$_2$] layer.

Cationic Arrangements. A two-dimensional supramolecular cationic layer was observed in the *ab*-plane of crystals **1**−**4** (Figure 4). The antiparallel arrangement of Ani$^+$ cations in

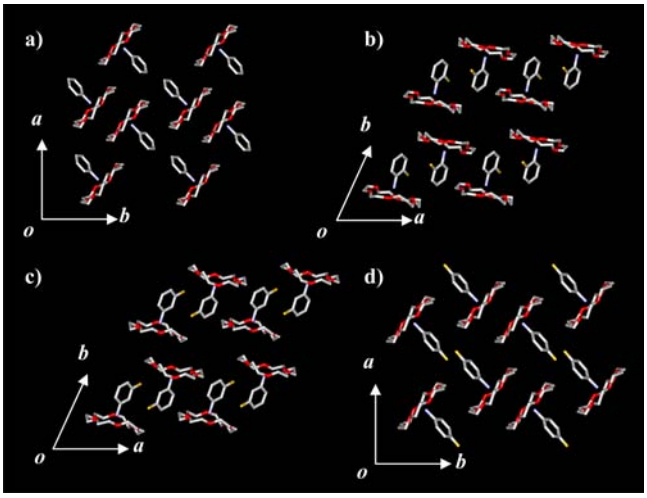

Figure 4. Supramolecular cation arrangement of crystals (a) **1**, (b) **2**, (c) **3**, and (d) **4** viewed along the *c*-axis. The cation arrangements of crystals **1** and **4** (group-**I**) were the same, whereas those of crystals **2** and **3** (group-**II**) were the same.

crystal **1** was observed along the *-a+b* direction. The neighboring [18]crown-6 molecules existed around the π-plane of the Ani$^+$ cation. The supramolecular cation arrangements of (*o*-FAni$^+$)([18]crown6) and (*m*-FAni$^+$)([18]crown6) in crystals **2** and **3** were the same. Fluorine substituents at the *o*- or *m*-position slightly modified the cationic arrangements along the *a*-axis. Since neighboring *o*-FAni$^+$ and *m*-FAni$^+$ cations were arranged in an antiparallel manner along the *a*-axis, the net dipole moment in the crystals was canceled. The rotation of *o*-FAni$^+$ and *m*-FAni$^+$ along the C-NH$_3^+$ axes was suppressed by the neighboring [18]crown-6 molecules. Similar isomorphous supramolecular cation arrangement in crystals **2** and **3** resulted in the same [Ni(dmit)$_2$] arrangements within the *ab*-plane.

The supramolecular cation arrangement of (*p*-FAni$^+$)([18]-crown-6) in crystal **4** was different from those of crystals **2** and **3**, and was the same to that of crystal **1**. The antiparallel arrangement of *p*-FAni$^+$ cations along the *-a+b* direction canceled the net dipole moment of the crystal. The neighboring [18]crown-6 molecules existed around the π-plane of the *p*-FAni$^+$ cation, forming a two-dimensional supramolecular cationic array. The same cationic arrangements in crystals **1** and **4** was the origin of the same [Ni(dmit)$_2$] arrangements within the group-**I** crystals.

Potential Energy Curves for Molecular Rotations. The molecular rotations of the phenyl- and fluorophenyl-ring along the C-NH$_3^+$ axis in crystals **1**−**4** were evaluated by potential energy calculation using the RHF/6-31(*d*) basis set.[11] Since the steric repulsions were the most important factors to determine the potential energy curves, the neighboring molecules were included in the calculations (Supporting Information, Figure S7). Several [18]crown-6 and [Ni(dmit)$_2$] molecules existed around the rotary units of aniliniums (see Supporting Information, Figure S7). The relative energies as a function of the rotational angle ϕ around the C-NH$_3^+$ axis of Ani$^+$, *o*-FAni$^+$, *m*-FAni$^+$, and *p*-FAni$^+$ cations were determined at every 30° rotation.

Figure 5a shows the rotational angle (ϕ) dependence of the relative energy (ΔE) of (Ani$^+$)$_3$([18]crown-6)$_3$, (Ani$^+$)$_2$([18]-

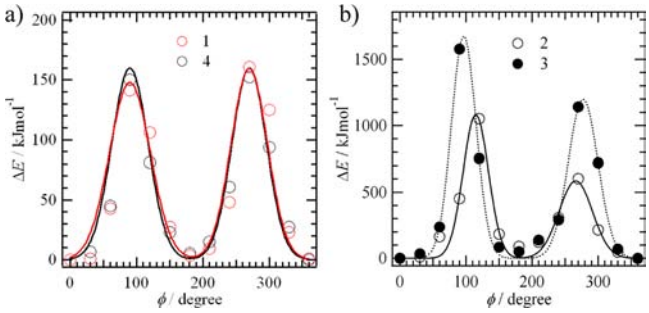

Figure 5. Rotational angle (ϕ) dependence of the relative energy (ΔE) of phenyl- and fluorophenyl-rings in the crystals. (a) ΔE vs ϕ plots of crystals **1** and **4** (group-**I**). (b) ΔE vs ϕ plots of crystals **2** and **3** (group-**II**). Calculated structures of crystals **1**, **2**, **3**, and **4** were (Ani$^+$)$_2$([18]crown-6)$_2$[Ni(dmit)$_2$]$_2$, (*o*-FAni$^+$)$_2$(DCH[18]crown-6)$_2$[Ni(dmit)$_2$], (*m*-FAni$^+$)$_2$([18]crown-6)$_2$[Ni(dmit)$_2$]$_2$, and (*p*-FAni$^+$)$_2$([18]crown-6)$_2$[Ni(dmit)$_2$]$_2$, respectively. The solid and dashed lines are included as a guide to the eye.

crown-6)$_2$[Ni(dmit)$_2$]$_2$, and (*p*-FAni$^+$)$_2$([18]crown-6)$_2$[Ni(dmit)$_2$]$_2$ in crystals **1** and **4** (group-**I**), where the relative energy at ϕ = 0° is defined as zero. For the rotational angle ϕ, the initial atomic coordinates from the X-ray crystal structure analysis corresponded to the first potential energy minimum at ϕ = 0°, while the second potential energy minimum was observed around ϕ = 180°. The double-minimum-type potential energy curves with two stable molecular orientations (ϕ = 0° and 180°) suggested 2-fold flip-flop motion of the phenyl- and *p*-fluorophenyl-rings in crystals **1** and **4**, which is the same as that in (Ani $^+$)([18]crown-6)[Ni(dmit)$_2$]$^-$.[8a] The magnitude of the potential energy barrier of crystal **1** (ΔE_{max} ∼ 150 kJmol^{-1}) was the same as that of crystal **4** (ΔE_{max} ∼ 150 kJmol^{-1}),[9] which were larger than that of (Ani$^+$)([18]crown-6)[Ni(dmit)$_2$]$^-$ (ΔE_{max} ∼ 40 kJmol^{-1}) and smaller than that of (*m*-FAni$^+$)(dibenzo[18]crown-6)[Ni(dmit)$_2$]$^-$ (ΔE_{max} ∼ 250 kJmol^{-1}). Symmetrical 2-fold flip-flop motion of the Ani$^+$ cation with a flip-flop frequency of ∼10^6 Hz was observed in the (Ani$^+$)([18]crown-6)[Ni(dmit)$_2$]$^-$ crystal at room temperature,[8a] whereas the 2-fold flip-flop motion of *m*-FAni$^+$ in the latter crystal yielded the ferroelectric-paraelectric phase transition at 346 K.[8e] From the magnitude of ΔE_{max} ∼150 kJmol^{-1}, the flip-flop motions of the Ani$^+$ and *p*-FAni$^+$ cations should be thermally activated around room temperature.

dx.doi.org/10.1021/ic302093b | *Inorg. Chem.* 2012, 51, 12968−12975

The rotational angle dependence of ΔE for crystals **2** and **3** (group-**II**) were significantly different from that for crystals **1** and **4** (group-**I**) from the viewpoint of rotational symmetry and height of the potential energy barrier. Asymmetrical double-minimum-type potential energy curves were observed in crystals **2** and **3**, whose potential energy barriers were larger than 600 kJmol^{-1}. Therefore, the rotations of *o*-FAni$^+$ and *m*-FAni$^+$ cations in the crystals were completely suppressed by the steric repulsions of neighboring molecules. The dynamic motion of Ani$^+$ and *p*-FAni$^+$ cations in crystals **1** and **4** (group-**I**) was suggested by the potential energy curves with relatively small ΔE_{max}, whereas the large magnitude of ΔE_{max} in crystals **2** and **3** (group-**II**) corresponded to the static nature of these crystals.

Electrical Conductivity and Magnetic Susceptibility. Table 3 summarizes the electrical conductivities and magnetic susceptibilities of crystals **1**−**4**. The electrical conductivities of crystals **1**, **2**, **3**, and **4** at 300 K were 2.86, 0.23, 0.26, and 6.1 S cm^{-1}, respectively. Figure 6 summarizes the log (σ/Scm^{-1}) vs T^{-1} plots of crystals **1**, **2**, **3**, and **4** measured along the π-stacking direction of the single crystals. The temperature-dependent electrical conductivities of all crystals showed semiconducting behavior with activation energies of 108, 99, 111, and 75 meV, respectively. Strong trimerization of [Ni(dmit)$_2$] in crystals **1**−**4** was consistent with the semiconducting temperature dependence.

Table 3. Electrical Conductivity and Magnetic Properties of Crystals 1−4[a]

	1	2	3	4
σ_{RT}, S cm^{-1} (T = 300 K)	2.86	0.23	0.10	6.1
E_a, meV	108	99	111	75
C, emu K mol^{-1}	0.29	0.376[b]	0.376[b]	0.25
J, K		−8.03	−11.5	
type[c]	M-NM	B. F.	B. F.	M-NM
g-value	2.02005	2.00167	2.05605	2.01875

[a]Single crystals using the four-probe method with 10 $\mu\phi$ gold wires along the π-stacking direction. [b]Fixed Curie constants. [c]The B. F. is a one-dimensional linear antiferromagnetic Heisenberg chain model. M-NM is a change in magnetic properties from the delocalized magnetic state to the non-magnetic state around 150 K.

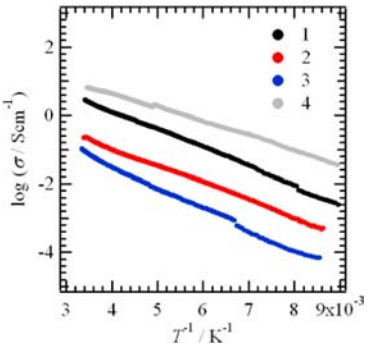

Figure 6. Log(σ/Scm^{-1}) vs T^{-1} (K^{-1}) plots of crystals **1** (black), **2** (red), **3** (blue), and **4** (gray) along the π-stacking direction of the single crystals.

Figure 7 shows the temperature dependent molar magnetic susceptibilities (χ_{mol} vs T) of crystals **1**−**4**. The χ_{mol} vs T plots of crystals **1** and **4** (group-**I**) resemble each other, whereas those of crystals **2** and **3** (group-**II**) show similar behavior. χ_{mol}-maxima of crystals **2** and **3** were observed at 10 and 16 K, respectively, the temperature dependence of which followed the one-dimensional linear antiferromagnetic Heisenberg chain.[14] The [Ni(dmit)$_2$] **A**-**B**-**C** trimer arrangements are a common structural feature of crystals **2** and **3** (see Figure 3c). The effective intertrimer t_4-interaction formed linear intermolecular interactions through lateral S∼S contacts between [Ni(dmit)$_2$] **B** and **B**′ anions. Since the magnitude of the intertrimer t_4-interaction between the lateral **B**-**B**′ pair is larger than the intertrimer t_3-interaction along the π-stack (**A**-**C**′ pair), a one-dimensional antiferromagnetic linear Heisenberg chain along the *a*-*b* axis is formed through lateral **B**-**B**′ interactions. The solid-lines in Figure 7b indicate fits using the one-dimensional antiferromagnetic linear Heisenberg chain model, where the magnetic exchange energies (J) of crystals **2** and **3** are −8.03 and −11.5 K, respectively, with a fixed Curie constant (C) of 0.376 emu K mol^{-1} per [Ni(dmit)$_2$]$_3$. Since the magnitude of the t_4-interaction in crystal **2** (t_4 = 47.2 meV) is smaller than that of crystal **3** (t_4 = 61.9 meV), the Weiss constant of crystal **2** was lower than that of crystal **3**, showing good accordance with $J \sim t^2/U_{eff}$ (U_{eff} is the on-site Coulomb repulsive energy on [Ni(dmit)$_2$] anion).[3]

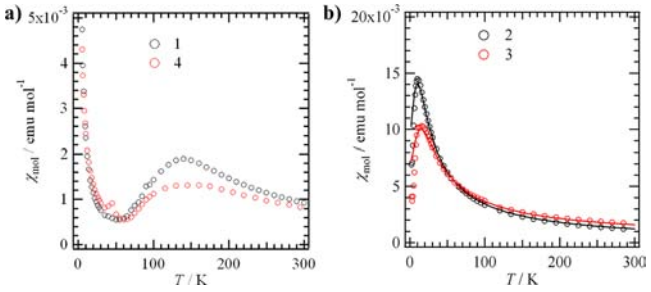

Figure 7. Temperature-dependent magnetic susceptibilities of crystals **1**−**4**. The χ_{mol} vs T plots of (a) crystals **1**, **4** (group-**I**) and (b) crystals **2**, **3** (group-**II**). The red- and black-lines are fits of the one-dimensional antiferromagnetic linear Heisenberg model.

The χ_{mol} vs T behaviors of crystals **1** and **4** (group-**I**) could not be explained by the simple one-dimensional antiferromagnetic linear Heisenberg model. A broad χ_{mol}-maxima around 150 K was observed in both crystals. The C-values of crystals **1** and **4** at 300 K were 0.29 and 0.25 emu K mol^{-1}, respectively, the magnitudes of which were smaller than those of crystals **2** and **4** and an ideal S = 1/2 spin system (0.376 emu K mol^{-1} per trimer). Figure 8 shows the σ vs T (left-scale) and $\chi_{mol}T$ vs T (right-scale) plots of crystals **1** and **4** (group-**I**). The σ-values of crystal **1** decreased monotonically by lowering the temperatures, where almost constant $\chi_{mol}T$-values of ∼0.30 emu K mol^{-1} were observed at temperatures above 150 K. When the electrical conductivity of crystal **1** almost disappeared at temperatures below 100 K, the magnetic spins also disappeared. In crystal **4**, the $\chi_{mol}T$-drop was consistent with the σ-drop at 150 K (Figure 8b). The low-temperature magnetic ground states of crystals **1** and **4** were non-magnetic states. One possible explanation for the non-magnetic ground states at low-temperatures in crystals **1** and **4** was the formation of strong intermolecular interaction between the (**A**-**B**-**C**) trimers. However, since the magnitudes of the intertrimer t_3- and t_4-interactions in crystals **1** and **4** were not drastically different from those of crystals **2** and **4**, a different mechanism is needed to explain the magnetic and conducting behaviors of crystals **1** and **4**.

dx.doi.org/10.1021/ic302093b | Inorg. Chem. 2012, 51, 12968−12975

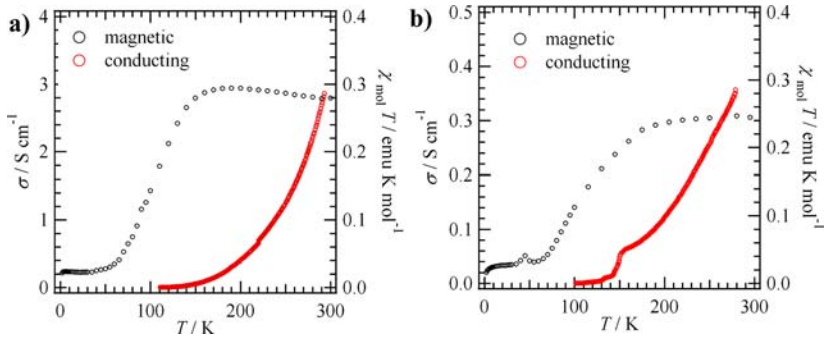

Figure 8. σ vs T (left-scale) and $\chi_{mol}T$ vs T (right-scale) plots of crystals (a) **1** and (b) **4**.

The χ_{mol}-values of crystals **1** and **4** at 300 K were ~1×10^{-3} emu mol^{-1}, slightly larger than the typical Pauli paramagnetism. The σ vs T behaviors were also in accordance with the semiconducting temperature dependences. When the electronic correlation between the conduction electrons was significantly strong, enhancement in the χ_{mol}-values from Pauli paramagnetism has been observed in molecular conductors. Another important difference between the two crystal systems (group-**I** vs group-**II**) was the difference in dynamic properties of the supramolecular cations. Thermally activated rotation of Ani^+ and *p*-$FAni^+$ cations was assumed in crystals **1** and **4**, whereas the rotation of *o*-$FAni^+$ and *m*-$FAni^+$ cations was prohibited from the large magnitude of the potential energy barriers. The periodic potentials for conduction electrons were modulated by the molecular rotations of the Ani^+ and *p*-$FAni^+$ cations in crystals **1**, which diffused electron localization. On contrast, the static polar cations of *o*-$FAni^+$ and *m*-$FAni^+$ in crystals **2** and **3** generated distinctive periodic potentials for the conduction electrons, which enhanced the electron localization potential. The differences in the motional freedom of supramolecular cations affected the electron localization-delocalization potentials within the $[Ni(dmit)_2]$ π-stacks, resulting in different $\chi_{mol}T$ vs T behaviors for group-**I** and group-**II** crystals.

The flip-flop motions of anilinium and *p*-fluoroanilinium were evidenced from the potential energy calculations, and the electrical conductivities of the crystals were quite significantly difficult to evaluate the molecular motions of Ani^+ and *p*-$FAni^+$ cations using the dielectric measurements (Supporting Information, Figure S7). However, the frequency- and temperature-dependences of the dielectric constants were observed at the temperatures above ~150 K. Thermally activated molecular rotations of Ani^+ and *p*-$FAni^+$ cations yielded the disordered crystal lattice and a diffuse periodic potential for the conduction electrons in the tight-binding model. When the thermally activated molecular rotations were suppressed by lowering of the temperatures, the periodic potentials of cationic arrangements are generated in the ordered state. Thermally activated conducting carriers on semiconducting $[Ni(dmit)_2]$ π-stacks should be affected by the order−disorder states of periodic potential for the conduction electrons. For the magnetic properties, the magnetic spins are generated by the localization of the conduction electrons. The molecular rotations within the $[Ni(dmit)_2]$ crystal lattice were coupled with the magnetic exchange energies through the modification of crystal lattice. For instance, the thermally activated molecular rotations of [18]crown-6 modified the magnetic exchange energy of $[Ni(dmit)_2]$ anions in $Cs^+_2([18]\text{-crown-6})_3[Ni(dmit)_2]_2$, resulting in the strange temperature-dependent magnetic properties.[7] The electrical conducting properties with partially oxidized electronic states of crystals **1** and **4** were also affected by the coupling with the molecular rotations, and magnetic spins were also influenced by the gradual conversion from conduction electrons to magnetic spins by lowering of the temperatures.

■ CONCLUSIONS

Supramolecular cationic assemblies of anilinium (Ani^+) and/or fluoroanilinium (F-Ani^+) derivatives with [18]crown-6 were introduced into electrically conducting $(Ani^+)([18]\text{crown-6})[Ni(dmit)_2]_3$ (**1**), $(o\text{-}FAni^+)([18]\text{crown-6})[Ni(dmit)_2]_3$ (**2**), $(m\text{-}FAni^+)([18]\text{crown-6})[Ni(dmit)_2]_3$ (**3**), and $(p\text{-}FAni^+)([18]\text{crown-6})[Ni(dmit)_2]_3$ (**4**) crystals, as counter cations. A cation:anion ratio of 1:3 yielded a partially oxidized electronic structure of $[Ni(dmit)_2]$, wherein the segregated cation−anion arrangements were observed in all crystals. The formation of a strong $[Ni(dmit)_2]$ π-trimer was confirmed by the calculations of transfer integrals. Each π-trimer was arranged in a two-dimensional layer through the lateral S~S contacts. The electrical conductivities at 300 K were observed to be 0.2−6 S cm^{-1}, and the semiconducting temperature dependencies were consistent with strong trimerization in $[Ni(dmit)_2]$ stacks. Although the $[Ni(dmit)_2]$ arrangements in crystals **1**−**4** were almost the same, the temperature dependent magnetic susceptibilities of crystals **1** and **4** were significantly different from those of crystals **2** and **3**. The one-dimensional antiferromagnetic linear Heisenberg chain was observed in crystals **2** and **3**, whereas the magnetic behaviors of crystals **1** and **4** showed a change in magnetic susceptibilities from a paramagnetic state to a diamagnetic one around 150 K. From calculations of potential energy curves for the molecular rotations of Ani^+, *o*-$FAni^+$, *m*-$FAni^+$, and *p*-$FAni^+$ cations along the C-NH_3^+ axis, thermally activated rotations of Ani^+ and *p*-$FAni^+$ cations were expected around room temperature. The delocalization behavior of π-electrons in the $[Ni(dmit)_2]$ layer in crystals **1** and **4** was governed by the rotation of Ani^+ and *p*-$FAni^+$ cations, whereas the static polar cations of *o*-$FAni^+$ and *m*-$FAni^+$ increased the localization property of π-electrons. The molecular rotations of cationic units are modulated, and they diffused the periodic potential for conduction electrons in the $[Ni(dmit)_2]$ stacks, which delocalized the conduction electrons. Further design of the supramolecular rotator in electrical conducting $[Ni(dmit)_2]$ crystals has the potential to modulate the electrical conducting behavior of molecular materials. Dipole inversion will largely affect the localization-delocalization property of the conduction electrons.

dx.doi.org/10.1021/ic302093b | *Inorg. Chem.* 2012, 51, 12968−12975

■ ASSOCIATED CONTENT

Supporting Information

Atomic numbering scheme, structural analysis of salts **1**−**4**, calculated model structures, vibrational spectra, UV−vis−NIR spectra, dielectric constants of crystals **1** and **4**, and nearest-neighbor packing of the rotators in crystals **1**−**4**. This material is available free of charge via the Internet at http://pubs.acs.org.

■ AUTHOR INFORMATION

Corresponding Author

*Phone: +81-22-217-5653 (T.A.). Fax: +81-22-217-5655 (T.A.). E-mail: akuta@tagen.tohoku.ac.jp (T.A.).

Notes

The authors declare no competing financial interest.

■ ACKNOWLEDGMENTS

This work was supported by a Grant-in-Aid for Science Research from the Ministry of Education, Culture, Sports, Science, and Technology of Japan, Management Expenses Grants for National Universities of Japan.

■ REFERENCES

(1) (a) Williams, J. M.; Ferraro, J. R.; Thorn, R. J.; Carlson, K. D.; Geiser, U.; Wang, H. H.; Kini, A. M.; Whangbo, M.-H. *Organic Superconductors*; Grimes, R. N., Ed.; Prentice-Hall: Englewood Cliffs, NJ, 1992. (b) Ishiguro, T.; Yamaji, K.; Saito, G. *Organic Superconductors*; 2nd ed.; Cardona, M., Fulde, P., von Klitzing, K., Queisser, H.-J., Eds.; Springer-Verlag: Berlin, Germany, 1998. (c) Kampen, T. K. *Low Molecular Weight Organic Semiconductors*; Wiley-VCH: Weinheim, Germany, 2010.

(2) (a) Miller, J. S.; Epstein, A. J. *Angew. Chem., Int. Ed. Engl.* **1994**, *33*, 385. (b) Miller, J. S.; Drillon, M. *Magnetism: Molecules to Materials*; Wiley-VCH: Weinheim, Germany, 2001. (c) Kahn, O. *Molecular Magnetism*; Wiley-VCH; Weinheim, Germany, 1993.

(3) (a) Scott, J. S. *Semiconductor and Semimetals. High Conducting Quasi-One-Dimensional Organic Crystals*; Conwell, E., Ed.; Academic Press: New York, 1988. (b) Torrance, J. B.; Scott, B. A.; Welber, B.; Kaufman, F. B.; Seiden, P. E. *Phys. Rev. B.* **1979**, *19*, 730.

(4) (a) Cassoux, P.; Valade, L.; Kobayashi, H.; Kobayashi, A.; Clark, R. A.; Underhill, A. E. *Coord. Chem. Rev.* **1991**, *110*, 115. (b) Pullen, A. E.; Olk, R.-K. *Coord. Chem. Rev.* **1999**, *188*, 211. (c) Robertson, N.; Cronin, L. *Coord. Chem. Rev.* **2002**, *227*, 93. (d) Kato, R. *Chem. Rev.* **2004**, *104*, 5319.

(5) (a) Nakamura, T.; Akutagawa, T.; Honda, K.; Underhill, A. E.; Coomber, A. T.; Friend, R. H. *Nature* **1998**, *394*, 159. (b) Akutagawa, T.; Hasegawa, T.; Nakamura, T.; Takeda, S.; Inabe, T.; Sugiura, K.; Sakata, Y.; Underhill, A. E. *Chem.—Eur. J.* **2001**, *7*, 4902. (c) Akutagawa, T.; Hasegawa, T.; Nakamura, T.; Inabe, T. *J. Am. Chem. Soc.* **2002**, *124*, 8903.

(6) Akutagawa, T.; Nishihara, S.; Takamatsu, N.; Hasegawa, T.; Nakamura, T.; Inabe, T. *J. Phys. Chem. B* **2000**, *104*, 5871.

(7) Akutagawa, T.; Shitagami, K.; Nishihara, S.; Takeda, S.; Hasegawa, T.; Nakamura, T.; Hosokoshi, Y.; Inoue, K.; Ikeuchi, S.; Miyazaki, Y.; Saito, K. *J. Am. Chem. Soc.* **2005**, *127*, 4397.

(8) (a) Nishihara, S.; Akutagawa, T.; Sato, D.; Takeda, S.; Noro, S.; Nakamura, T. *Chem.—Asian J.* **2007**, *2*, 1983. (b) Sato, D.; Akutagawa, T.; Takeda, S.; Noro, S.; Nakamura, T. *Inorg. Chem.* **2007**, *46*, 363. (c) Akutagawa, T.; Sato, D.; Koshinaka, H.; Aonuma, M.; Noro, S.; Takeda, S.; Nakamura, T. *Inorg. Chem.* **2008**, *47*, 5951. (d) Akutagawa, T.; Nakamura, T. *Dalton Trans.* **2008**, 6335.

(9) Akutagawa, T.; Koshinaka, H.; Sato, D.; Takeda, S.; Takahashi, H.; Kumai, R.; Tokura, Y.; Nakamura, T. *Nat. Mater.* **2009**, *8*, 342.

(10) (a) *Crystal Structure: Single crystal structure analysis software*, Ver. 3.6; Rigaku Corporation and Molecular Structure Corporation: Tokyo, Japan, 2004. (b) Sheldrick, G. M. *SHELX97 Programs for Crystal Structure Analysis*; Universitat Göttingen: Göttingen, Germany, 1998.

(11) Frisch, M. J. et al. *GAUSSIAN R03W*; Gaussian, Inc.: Pittsburgh, PA, 2003.

(12) Mori, T.; Kobayashi, A.; Sasaki, Y.; Kobayashi, H.; Saito, G.; Inokuchi, H. *Bull. Chem. Soc. Jpn.* **1984**, *57*, 627.

(13) (a) Jeffrey, G. A. *An Introduction to Hydrogen Bonding*; Truhlar, D. G., Ed.; Oxford University Press: New York, 1997. (b) Pimentel, G. C. McClellan, A. L. *The Hydrogen Bond*; W. H. Freeman: San Francisco, CA, 1960.

(14) Carlin, R. L. *Magnetochemistry*; Springer-Verlag; Heidelberg, Germany, 1986.